The International Journal of Advanced Manufacturing Technology
https://doi.org/10.1007/s00170-025-16810-2

ORIGINAL ARTICLE

High-accuracy real-time controlled robotic-based bioprinting onto unknown and moving surfaces

Andrea Guerra[1,2] · Shakiba Davani[3] · Carlo Usai[1,2] · Tomasz Jüngst[4] · Christos Boutopoulos[3] · Gabriele Maria Fortunato[1,2]

Received: 26 June 2025 / Accepted: 12 October 2025

Abstract
This study aims at developing a robotic bioprinting system capable of detecting and compensating for unexpected movements or irregularities of the printing substrate in real time, thus achieving high-accuracy deposition. To this end, a fiber-optic distance sensor based on spectral domain optical coherence tomography was integrated on a commercial anthropomorphic 6-axis robot. The sensor provides a continuous signal, which is used in a feedback control system developed in Python. This system dynamically adjusts the position of the end-effector according to the distance from the printing plane, keeping it constant. The entire setup was validated by executing printing tests (planned with simple planar trajectories) on both moving and stationary non-planar substrates with *a priori* unknown surface geometry. Real-time controlled printing tests proved the functionality of the developed system, showing smooth results in different scenarios while highlighting significant advantages of the proposed approach against procedures without compensation. The end-effector positioning accuracy and the average printed line width deviation resulted lower than 100 μm, thus proving the high compatibility with bioprinting applications. This approach lays the technological foundations for possible future applications of both *in situ* bioprinting, where physiological movements of the patient, such as breathing, heartbeat or tremors, hinder the accuracy of the deposition, and *in vitro* bioprinting, where substrates often have surface irregularities that compromise the quality of the final result and used soft materials tend to collapse when considering large size constructs. Moreover, the proposed method guarantees the reduction of the path planning computational cost since it can adapt any printing system to complex surfaces, even when starting from planar trajectories.

Keywords Real-time controlled bioprinting · Robotic-based bioprinting · Optical Coherence Tomography based distance sensor · Fiber sensor · Unknown and moving printing surface

1 Introduction

Bioprinting is a field of Tissue Engineering (TE) that uses additive manufacturing (AM) technologies [1] to create living tissues or potentially entire organs, by depositing layer by layer a mixture of cells, biomaterials, and biomolecules (*i.e.,* bioink) [2–5]. Standard bioprinting techniques, which involve creating the 3D construct *in vitro* and then grafting it into the human body [2, 6, 7], have intrinsic limitations due to the printers' characteristics and the maturation process [8]. Tissue defects resulting from disease or trauma typically have an irregular morphology, and structures printed on flat surfaces with conventional Cartesian bioprinters cannot easily conform to this complex geometry [8]. Furthermore, after the construct has been cultured *in vitro*, it can deform, making it difficult to graft it into the patient's body and requiring secondary fixation methods [8, 9]. Moreover, another limitation of the conventional 3D bioprinting process is the slow speed in meeting the most urgent clinical needs. In the case of a traumatic injury, it takes several hours to acquire 3D images of the injury site, reconstruct the CAD (computer-aided design) model to be printed and perform the printing. Furthermore, when the scaffold is ready, a second surgery is often necessary that exposes the patient to new risks of infection, delays treatment, and potentially reduces the regenerative properties of the remaining tissue [8]. Faced with these limitations, *in situ* bioprinting is an approach that involves direct bioprinting of the bioink inside the defect, with a print that conforms to complex tissue surfaces [8, 10, 11]. In this way, the treatment can be applied immediately, and the procedure can be

Extended author information available on the last page of the article

Published online: 20 October 2025

monitored in real-time, reducing the duration and minimizing issues related to changes in the defect microenvironment caused by the dynamic nature of wounds or surgical resection [8, 12, 13]. Furthermore, the adhesion of the scaffold to the residual tissue is improved through *in situ* cross-linking, increasing tissue-scaffold integration [14, 15]. Finally, the body, acting as a natural bioreactor, is far superior to *in vitro* culture conditions for tissue regeneration and reduces the possibility of contamination [10, 16]. *In situ* bioprinting can be handheld or robotic. The first uses devices that can easily be held by an operator, and the material is deposited directly on the patient site without the need for defect scanning and path planning through geometry slicing. This approach offers surgeons considerable freedom, allowing them to quickly stop and/or restart the printing process on demand, as well as allowing for any potential patient movement during surgical procedures. On the other hand, this approach brings limitations inherent to human nature: limited repeatability, low accuracy, low precision, presence of errors related to the natural tremor of the surgeon's hands, or unwanted movements due, for example, to breathing. On the other hand, robotic-based *in situ* bioprinting is the most promising approach since it can greatly facilitate the process, ensuring high precision and repeatability in a fully automated context where human intervention is minimized [17, 18]. Articulated robots are the most used configuration, as they offer the workspace and degrees of freedom (DOF) needed to print inside body defects regardless of their geometric complexity and anatomical position [19, 20]. The redundancy of DOF can be exploited to improve manipulability and achieve more dexterity, to use advanced kinematic control algorithms that improve movement precision, and to allow the structure to unfold/fold to reduce its bulk [21]. Finally, articulated robots integrate the possibility of using different printing technologies to adapt to the type of defect and patient tissue [13, 22–24]. Among the first works is that of Li et al. [12] where the efficacy of using a 6-DOF industrial robot for *in situ* bioprinting was demonstrated by depositing a bioink based on sodium alginate, polyethylene glycol diacrylate (PEGDA), and gelatin methacrylate (GelMA) in animal models. Subsequently, Zhao et al. [25] used a 6-DOF robot equipped with scanning tools for the rapid reconstruction of skin defects, further demonstrating the need for multi-DOF platforms to effectively cover large defects. In a recent work, instead, a 5-DOF robotic platform for *in situ* bioprinting was developed, exploiting its dexterity to enable non-planar printing on the irregular surfaces of human tissues and verifying the possibility of integrating multiple printing technologies in a single process.

The bioprinting process typically involves an initial phase in which the trajectories are planned based on the geometry of the defect or tissue to be created, which can be known *a priori* or acquired through surface reconstruction techniques [26, 27]. A limiting aspect of this approach, however, is the actual possibility of planning a printing path that can faithfully follow the profile of the tissue [28]. The human body is an extremely dynamic environment that, in addition to being characterized by irregular surfaces, has intrinsic movements, such as heart rate, breathing, or even changes in the tissue microenvironment of the defect, which cannot be eliminated [28–30]. The movement of the substrate must be considered to guarantee, on the one hand, the safety of the patient, and on the other, the possibility of printing on all body tissues and not only on rigid or immobilized ones [8, 29]. Furthermore, the irregularity of the surface, combined with the natural presence of liquids in human tissues, often means that scanning techniques are unable to capture all the geometric characteristics [27]. This happens because the damaged site may not be easily accessible to the scanning tool, liquids can interfere with the reconstruction technology, or the tool has a limited intrinsic accuracy [28, 31, 32]. Therefore, the need arises to be able to print on non-planar, irregular surfaces, with possibly unknown geometry and in motion. Being able to implement a technology of this type would have implications in different sectors, in addition to the medical one, as in mobile environments such as ships, and vehicles, or, for 3D printing in space stations, where frequent attitude checks generate transient vibrations and involuntary movements that make the procedure more challenging [33, 34]. In all these cases, on-site printing may be the only solution, given the lack of proper scanning systems or the need to quickly repair objects and instruments that cannot be moved. To achieve this goal, in addition to non-planar path planning methods, it is necessary to use feedback systems that allow monitoring and maintaining the relative position of the substrate-tool constant even in the absence of a precise geometric description of the object or in the presence of unexpected movements [35, 36]. In a recent study, Fortunato et al. implemented a compensation system in an *in situ* bioprinting platform to balance the physiological movements of the patient [30]. The system made it possible to compensate for a periodic movement of the patient (for example, a beating heart, a movement of the thoracic cavity induced by breathing) or to interrupt the bioprinting process following a sudden and unexpected movement. However, the compensation was not in real-time but was based on the acquisition of the movement before the printing phase: the frequency and excursion of the movement were stored and then added to the printing trajectories in the inverse kinematics calculation phase. Among the first works that exploit real-time information detection is that of Armstrong et al. [37] who created a real-time feedback system to improve the quality of the print by monitoring the spatial positioning of the deposited material with respect to the desired position. The only goal in this case was to improve the spatial resolution of the bioprinting and did not include adaptation to move-

ments or irregular surfaces. To allow direct process control and measure deposition, a laser profiler (Keyence LJ-G030) was mounted on the extruder head. On the other hand, to print on moving surfaces, O'Neill et al. in 2017 [29] introduced an optical tracking algorithm to detect the anatomy pose in real-time. A Leap Motion tracking system (framerate 120 Hz, resolution 1 mm) was used for XY tracking, while a custom profiler made with a linear green laser (532 nm, 1 mW) and a Raspberry Pi hardware camera were used for Z. A Cartesian printer was used to accurately position the nozzle relative to the substrate. The nozzle's movement was adjusted at a speed proportional to the positioning error along the X, Y, or Z axes. However, this method required pausing the material extrusion until the nozzle was correctly repositioned. Subsequently, Zhu et al. [36] created a system capable of detecting in real-time the movements of the substrate and adapting the printing accordingly. The process involves first a structured light scan of the surface, then the combination of the geometric information obtained with a real-time estimation of the body's movement. The movement is detected by stereo cameras mounted on the robot's end effector, which allows the use of the Prospective-n-Point (PnP) method to locate the fiducial markers placed on the moving surface. To be detectable, however, the movements must have a linear speed lower than 8 mm/s. Nevertheless, all the analyzed systems have the limitation of being based on image acquisition and processing, resulting in high-dimensional data that necessarily involve a high computational cost and a non-negligible time for generating the feedback signal. Furthermore, these methods require a global description of the object's surface, which is not always obtainable. Other studies have found simpler solutions from a computational point of view, but equally effective, because they directly act on maintaining the correct height offset between the substrate and the extruder. Kucukdeger et al. [38] implemented a feedback system based on a 1D laser displacement sensor to monitor and maintain constant the offset between the substrate and the nozzle. The laser sensor (IL-030, resolution 64 μm) was mounted on a 3-axis Cartesian printer adjacent to the extruder, moved by 0.1 mm in the X direction (distance selected to capture the movement of the next point of the tool path while avoiding interference from the extruded material). The implemented system demonstrated the ability to mitigate the effect only in the case of displacements lower than 4 mm. Furthermore, the use of a Cartesian printer limits the applicability of the system only to easily accessible regions of the body and with not very complex geometries. A similar work was proposed by Levin et al. in 2023 [39]. In this case, an end effector was created for the KUKA Sunrise Cabinet robot, equipped with a VL53 time-of-flight (ToF) distance sensor and a stepper motor for real-time modification of the position of the print head. Although the system allowed easy control of the position of the nozzle, the sensor guaranteed a poor resolution ($>$ 1 mm), limiting the effective possibility of use in *in situ* bioprinting applications.

To overcome these limitations, this study integrates a position feedback system on a commercial 6-DOF articulated robot. The system monitors the distance between the nozzle and the printing substrate in real-time and keeps it constant, allowing both to compensate for physiological or unexpected movements of the patient and to print on complex surfaces with unknown geometry. The distance detection is performed by using a fiber-based distance sensor based on spectral domain Optical Coherence Tomography (OCT). The position update was validated either by acting directly on the kinematic chain of the robot or by using an actuated tool as an end-effector, capable of controlling the position of the nozzle.

2 Materials and methods

2.1 Overview of the proposed method

In this study, we implemented a real-time position control to increase the accuracy of robotic-based bioprinting, also when printing onto moving and/or *a priori* unknown surfaces. As shown in Fig. 1 a, our approach involves the use of a distance sensor installed on the end effector of the robot (pneumatic extrusion-based bioprinting system) that constantly measures the distance d from the print substrate in real-time with the aim of maintaining a constant distance h between the print nozzle and the substrate. By setting a fixed threshold d in the robot control algorithm, when the sensor measures a value $> d$, the robot will move downwards (decreasing the z-coordinate of the end effector position), and vice versa in the case of a measured value $< d$. This approach considerably reduces the complexity of trajectory planning, as it is possible, starting from a planar path (reduced computational cost of determining the coordinates of the points of the trajectory), to successfully complete the following procedures:

- printing on an unknown surface (Fig. 1b): the robot adapts to any substrate by adjusting its z-position in real-time while maintaining a constant distance from the substrate;
- printing on a moving and/or deforming surface (Fig. 1c): the robot follows the movement of the substrate (*e.g.,* in the case of *in situ* bioprinting, physiological movements of the patient such as heartbeat and breathing activity) thanks to the distance feedback.

In addition to the previous applications, our approach could also allow for improved accuracy during bioprinting of soft materials. In these cases, in fact, especially when considering large construct sizes ($> 5mm$), the weight of the upper layers, weighing down on the lower ones, can lead

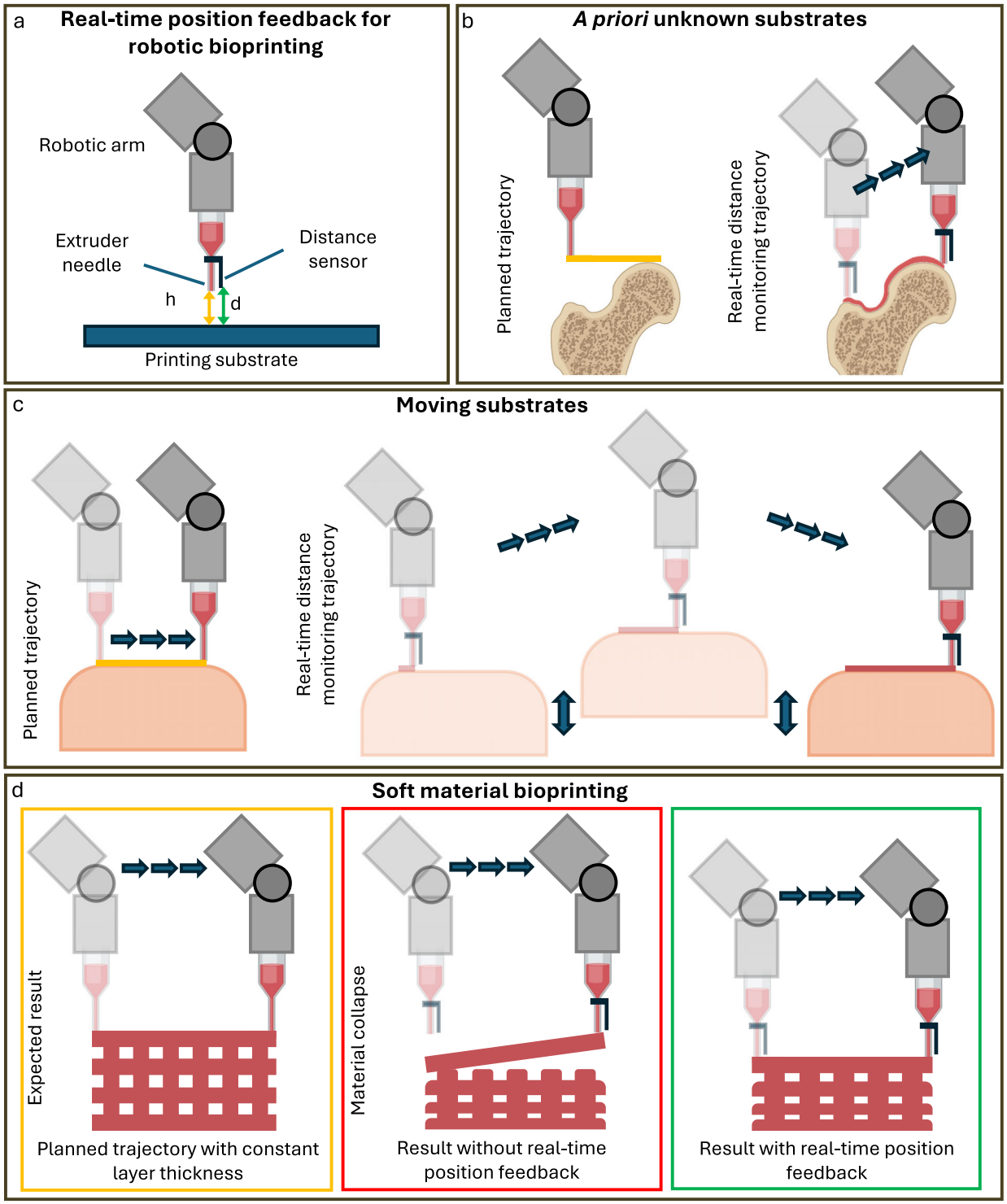

Fig. 1 Overview of the proposed real-time position-controlled robotic-based bioprinting: a) Graphical representation of the position-feedback approach: a distance sensor is installed on the robot end-effector (*i.e.,* pneumatic extruder) and measures, in real-time, the distance d from the substrate to maintain a constant distance h between the needle and the printing substrate. – b) Starting from a planar planned trajectory, the robot adapts the end-effector z-position to follow a priori unknown complex and curved geometries thanks to the distance feedback. – c) Starting from a planar planned trajectory, the robot can follow the movement and/or the deformation of the substrate, adapting the end-effector z-position. – d) Due to soft material collapse in high constructs, the distance feedback allows to always deposit the material at the correct height

to a collapse of the structure and thus a change in the total height expected at the n-th layer. When this happens, the planned trajectory at the height $n \times$ *layer height* will lead to the deposition of the material at an unacceptable distance from the layer below, not allowing the planned geometry to be realised correctly. Following the proposed approach, the constant distance feedback allows the robot to position itself at each layer change, and during the execution of the layer itself, always at the correct z-position to maintain a constant thickness. For real-time controlling the position of the end effector, we present two different approaches in this study. The first allows the position of the robot to be controlled directly, through a real-time update of the joint angles (Fig. 2a). The second is based instead on the use of an actuated end-effector, in which an additional prismatic degree of freedom (DoF) allows the z-position of the extrusion system to be adjusted to follow the distance feedback from the sensor (Fig. 2a). The latter approach also makes it possible to implement the proposed method on 3D printers and robotic arms that do not allow for real-time kinematics updating. In both cases, the z-displacement applied will be proportional to the difference between the desired (*i.e., d*) and the measured distance.

2.2 OCT-based sensor

The distance sensing automation was built using a home-made spectral domain common-path OCT system and a fiber-based OCT probe. The system employs a SLED light source (central wavelength: 880 nm; bandwidth: 70 nm, EXS210088-02; Exalos, Schlieren, Switzerland) powered by a compact driver board (EBD 5020; Exalos), a spectrometer (AvaSpec-ULS4096CL-EVO; Avantes, Apeldoorn, the Netherlands), a 50:50 fiber coupler (AC Photonics Inc., Santa Clara, CA, USA), and a variable optical attenuator (V800A; Thorlabs). A Matlab® program was used to control the system. A 2-meter-long fiber (SM800-5.6-125, Thorlabs) was used as the basis for the probe. To optimize light emission and collection from the fiber, we spliced a 272-μm GRIN fiber (GIF625) to its distal end, resulting in a non-diverging light beam emission [40]. The fiber probe was attached to the end effector, emitting light towards the moving and/or unknown printing substrates (Fig. 2 b). The scattered light was collected from the same fiber probe and directed to the spectrometer. We processed the signal collected by the spectrometer (interferogram) using Matlab® and a standard signal processing approach in OCT [41]. First, evenly spaced wavelength data were converted into evenly spaced k-space data using linear interpolation. Then, an inverse Fourier transform was applied, converting the interferogram into distance-resolved intensity (A-scan). Any back-reflecting object placed into the beam path manifested as a sharp peak in the A-scan, with the x-position of the peak representing the distance of the object from the fiber sensor tip. To extract the real-time distance (70 Hz) of the moving and/or unknown printing substrate, the position of the peak was interrogated in real time using the max function in Matlab® within the 80 μm to 1000 μm range. The axial resolution and working range of the system were experimentally measured to be 18 μm and 1500 μm, respectively, using a microscope slide as the target. However, the actual working distance for common low-reflecting samples, such as the biomaterial ink and PLA substrates used in this work, was shorter ($\sim$ 1000 μm).

2.3 Design of robotic platform

The robotic platform used in this work is the 6-axis MECA500 (Mecademic, Canada). The selected commercial system ensures a high positioning repeatability (about 5 μm) and resolution (about 1 μm) in a compact architecture, therefore ideal for bioprinting applications where an accuracy of less than 100 μm is required. The serial communication available on the platform allows easy integration with other systems/sensors. Moreover, the robot can be operated either through the MecaPortal web interface (which offers both control via code and a remote operation mode) or through Python, C++, C# and LabVIEW scripts for more customised applications. In Python, the robot can be controlled using the PyAutoGUI library, which allows more advanced workflows to be developed than the online interface allows. The actuated tool to be installed as an end-effector of the MECA500 was designed using the CAD software Autodesk® Fusion 360. It is composed of a fixed and a moving element, respectively. In the fixed one, two parts can be identified: the bottom part, attached to the robot end-effector by a magnetic plaque, houses a servo motor and one of the pulleys, and a top part linked to the previous one, which houses the second pulley and limits the possible range of movement of the reservoir (*i.e.,* 5 ml syringe). The moving element holding the syringe is driven by a belt-pulley mechanism. Two steel rods allow the translation and give the tool the proper mechanical stiffness (Fig. 2c). The tool design takes into consideration a few key elements: i) it should occupy as little space as possible after the end-effector of the robot not to reduce its workspace. For this reason, the servo motor (Miuzei MZ996) was positioned immediately after the wrist of the robot and most of the tool was positioned at its side, with enough distance to allow it to fit both on the front and on one side (this was also necessary to avoid any collision if the path planning calls for the turning of the wrist); ii) the syringe was positioned aligned to the robot's wrist axis to easily identify its reference frame for path planning; iii) the point of the belt that transmits the movement to the moving part has to be central to avoid any jamming; iv) the moving part has a possible range of motion of 28 mm, allowing printing on non-planar and/or moving surfaces; v) in the highest position of the moving

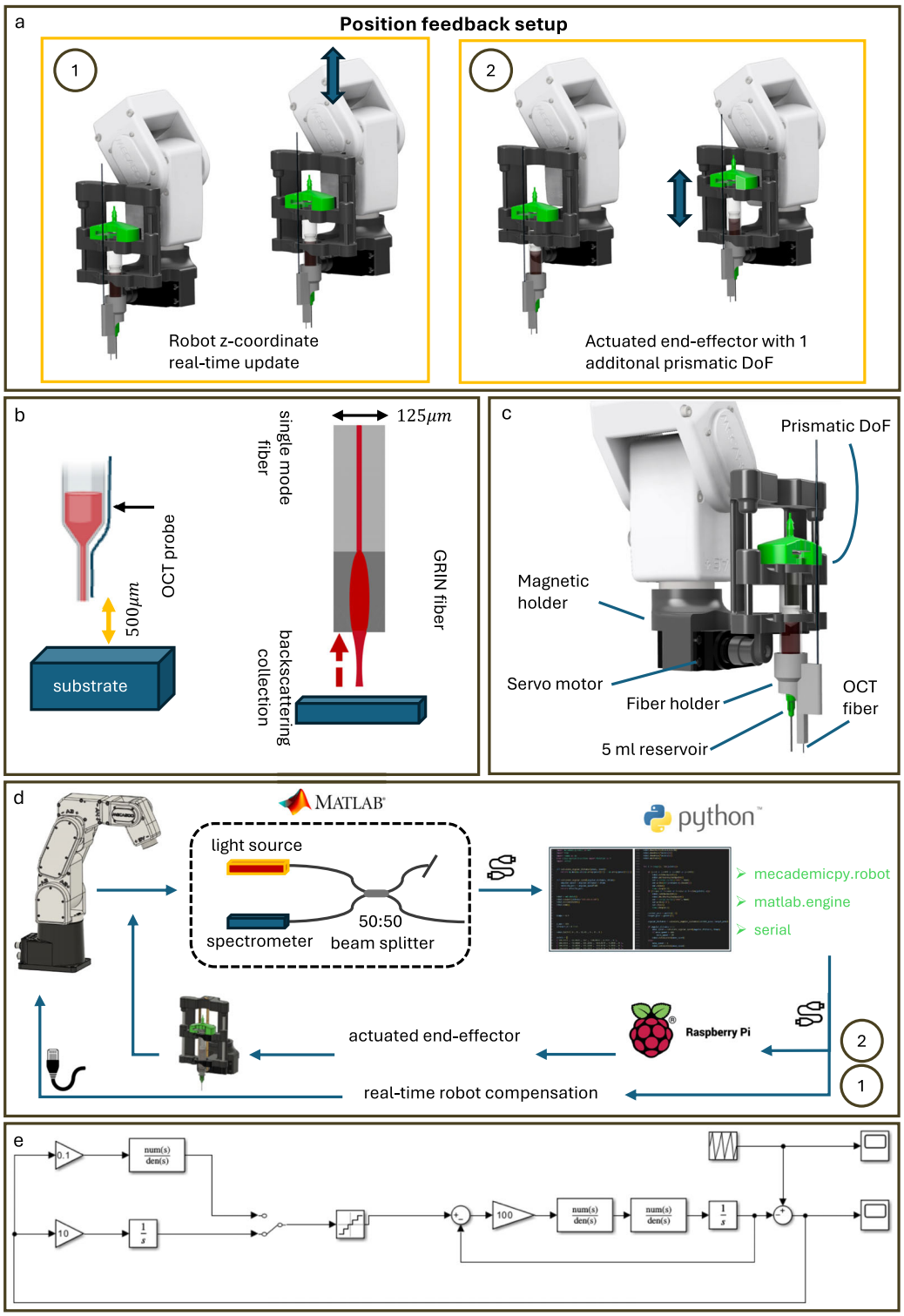

Fig. 2 a) Overview of the position feedback setup: in 1 the z-position of the robot is real-time updated by adjusting joint angles according to the distance measured from the sensor; in 2 the z-position of the end-effector is adjusted using an actuated tool with an additional prismatic DoF; - b) Left: Integration of an OCT fiber probe with the printing nozzle, maintaining a 500 µm distance between the fiber tip and the substrate. Right: Schematic of the OCT distance probe consisting of a single-mode fiber and a GRIN fiber; - c) Design of the robotic arm end-effector: actuated extrusion-based unit driven by a servo motor and a belt-pulley mechanism. The OCT fiber is kept in place as close as possible to the printing nozzle through a purposely designed holder; - d) Real-time position feedback protocol following two different approaches 1 and 2 – e) Implemented Simulink® model

element a gap with the top part of the fixed element allows avoiding any collision of the syringe pneumatic adapter. The 3D model was 3D printed in Acrylonitrile Butadiene Styrene (ABS) using the commercial 3D printer Stratasys^{TM} F370.

2.4 Matlab-Python interface

The acquisition and extraction of the distance signal provided by the OCT sensor is performed via a Matlab® script (see Section 2.2), while the control of the robot and the actuated tool (Fig. 2a) is carried out via Python and Arduino scripts, respectively. For this reason, a strategy was implemented to establish a real-time communication channel between the Matlab® environment, in which the distance variable is constantly read and updated, and the Python or Arduino environment, in which the same variable must be known in order to allow a proper positioning control (Fig. 2d). In the case of real-time control of the robot, communication occurs by importing into the Python script the *matlab.engine*, a module of the *MATLAB Engine API for Python* library that allows scripts to be executed, functions to be called, and Matlab® workspace variables to be accessed directly from Python. Specifically, the $eng = matlab.engine.start\_matlab()$ command is used to create a background instance. Once instantiated, the *eng* object contains many methods specific to:

- perform operations; for example, $eng.eval('y=5 \hat{} 2;', nargout = 0)$ allows the operation to be calculated using Matlab® as the calculation engine;
- execute scripts; the command $eng.my\_script(nargout = 0)$ allows you to execute the script $'my\_script.m'$ stored in the same directory as the Python script;
- access the variables stored in Matlab® workspace with the command $x = eng.workspace['var']$.

Thus, to have the new distance value read from the OCT sensor and processed in Python in Matlab, it was sufficient to execute the following commands in the Python script:

$$eng.sensor\_data(nargout = 0)$$
$$distance = eng.workspace['OCT\_distance']$$

Once the data is acquired, it is used to update the kinematic configuration of the robot in order to keep the relative z-coordinate of the end effector constant at a pre-defined value. This distance was set to 500 μm, which corresponds to approximately 2/3 of the nozzle inner diameter (830 μm). This choice is consistent with common practice in hydrogel bioprinting, where the layer thickness is typically set to 60–70% of the nozzle diameter, in order to ensure adequate inter-layer adhesion while avoiding both excessive spacing between layers and undesired nozzle contact with the previously deposited filament. In particular, the current 'distance' read from Matlab® workspace is subjected to an initial filtering: if it is greater than 1000 μm or in the range between 450 and 550 μm, the robot's coordinates are not updated. This is because, in the first case, a distance greater than 1000 μm is associated with a reading error of the sensor (which can acquire the signal up to a maximum distance of 1000 μm), while, in the second case, activating the robot to compensate for deviations of only 50 μm leads to oscillations and difficulties in stabilizing around the target distance. If the read distance is correct, on the other hand, the deviation (increase) from the target distance of 500 μm is calculated, and the z-coordinate $'current\_z'$ of the end effector is updated as follows:

$$increase = round(0.5 * ((500 - distance) * 1e - 3), 2)$$
$$current\_z+ = increase$$

The additive update of the z-coordinate introduces an implicit integrative effect on the state variable, while the error itself is not explicitly integrated. This implies that the control law can be considered as a P (proportional) controller, since the correction term is directly proportional to the instantaneous error. If d* is the desired distance, d[k] is the measured distance at step k, e[k]=d*-d[k] is the error, and z[k] is the offset applied to the robot in mm, then the P control has the following form:

$$\Delta z[k] = Kp \cdot e[k]$$
$$z[k+1] = z[k] + \Delta z[k]$$

with $Kp = 0.5$. The value has been calibrated following preliminary tests and allows the distance to be corrected smoothly, thus avoiding excessive oscillations and overshoot (the nozzle getting too close to the substrate, risking collision).

In the case of actuated tool control, on the other hand, the dedicated servomotor is controlled with a Raspberry Pi Pico control board on which an .ino firmware developed in the Arduino IDE is loaded. In this case, the serial port is used to establish communication between the Matlab® and the Arduino environment. In particular, after reading the distance in Matlab® , the serial port to which the Pico is connected is defined, an object of type serial is instantiated, and communication is initiated, as follows:

$$serialPort = 'COM11';$$
$$picoSerial = serial(serialPort, 'BaudRate', 115200, 'Terminator', 'LF');$$

At this point, for each new distance value read from the OCT sensor, it is first converted to a string with the Matlab® func-

tion $data = sprintf('<\%d>', OCT\_distance)$ and then sent to the serial with the function $fprintf(picoSerial, '\%s', data)$. On the other hand, the firmware loaded on the Raspberry Pi Pico allows it to read the data received via the serial with the $Serial.read()$ command, and then receives the current distance value detected by the sensor. Once the value has been received, similarly to real-time robot control, the deviation from the target distance is calculated. This deviation corresponds to a translation, which is converted into an angular value sent to the servo motor with the command $servo.write(increaseAngle)$.

2.5 Experimental validation

Different printing tests were carried out to validate the developed system, exploiting the two approaches previously detailed. In all tests, a planar serpentine trajectory was executed with a constant linear speed of 4 mm/s. 20% w/v Pluronic Acid F127 (Sigma-Aldrich, Italy) was used for all the bioprinting experiments, using a 18G needle (Metcal, Italy) and applying a 0.45 bar pressure. Speed and pressure were optimized for the used material and were selected following a preliminary printing test on a static printing substrate to ensure the deposition of a homogeneous line. Environmental conditions were kept constant throughout all experiments (temperature 25°C and humidity 30%) so as not to alter the rheological properties, and therefore the printing accuracy, of the selected material. 20% w/v Pluronic F127 is stable above 20°C, while it begins its transition to a liquid state at temperatures below 18°C.

For both setups, the serpentine was printed on four different surfaces: a glass slide that is moved up and down by a servo motor controlled by an Arduino Mega board with a maximum displacement of 15 mm and a period of 11 seconds, and three different stationary 3D printed surfaces, two made of polylactic acid (PLA), each with a different colour (blue and black) and geometry, and a transparent Petri dish with a curved bottom. An additional test was also performed by printing the same model into a commercial Petri dish. Printing tests onto moving substrates were also repeated without real-time position compensation. Each trial was performed in triplicate. During each test, the measured distance with the OCT-based sensor was registered and compared with the set threshold (500 μm). To obtain more accurate values, the acquired signal was subjected to adaptive filtering using the Total Variation Denoising algorithm via Matlab® . The line width of the serpentine was also measured on the acquired images using the software ImageJ®. The accuracy of the proposed method was quantified by comparing the values of the measured line width with the internal diameter of the needle used. Collected data of distance and line width were analysed with a one-way analysis of variance (ANOVA) using the software GraphPad prism 10.2. Results are reported as mean ± standard deviation. To qualitatively analyze the position outputs, a Simulink® model of the system was developed to estimate its dynamic behavior. The robotic arm was represented by a third-order closed-loop system employing purely proportional control. The external control mechanism was modeled as an integral closed-loop system. A quantization block, operating at the same sampling frequency as the distance sensor, was introduced between the external controller and the robotic arm to simulate the effects of digital discretization. The sawtooth motion of the printing substrate was used as the reference signal to be tracked.

3 Results and discussion

3.1 Experimental validation with real-time robot compensation

The real-time adaptation of the robot's kinematics to follow the displacement of the substrate was successfully achieved, resulting in regular and homogeneous prints that resulted not feasible without activating the compensation system (Fig. 3a). Pictures were acquired at the end of each printing test, and images were analysed using ImageJ software. It was observed that the printed serpentines had a line width of 0.85 ± 0.09 mm (needle inner diameter = 0.83 mm) with no statistically significant differences between the three trials (p-value > 0.05). When the same trajectory was executed on a moving substrate without motion compensation enabled, the resulting serpentines were discontinuous, showing clear segments without extrusion due to the excessive distance from the substrate (Fig. 3b).

Comparing the time trend of the substrate position with that of the nozzle-substrate distance measured during printing with compensation (Fig. 3c) it was observed that: (i) during the downward movements of the substrate (*i.e.,* 'moving away' from the nozzle), a 'tracking' mechanism is triggered by the robot, which keeps the nozzle at an average distance of 640 μm; (ii) during the upward movements of the substrate (*i.e.,* 'approaching' the nozzle), a 'fleeing' mechanism is triggered, and the nozzle is kept at an average distance of 420 μm. The robot is therefore able to follow the movements of the substrate despite the presence of small offsets from the desired distance, which, however, do not compromise the quality of the print. These offsets are due to the implementation of a P control (see Section 2.4). The results of the Simulink® model confirmed what was observed experimentally (Fig. 3d), showing a positive or negative deviation depending on the direction of the substrate.

The overall closed-loop system is a type 1 servo that exhibits a constant tracking error in steady-state conditions when the reference is a ramp signal. Discretization introduces additional chattering in the steady-state behaviour.

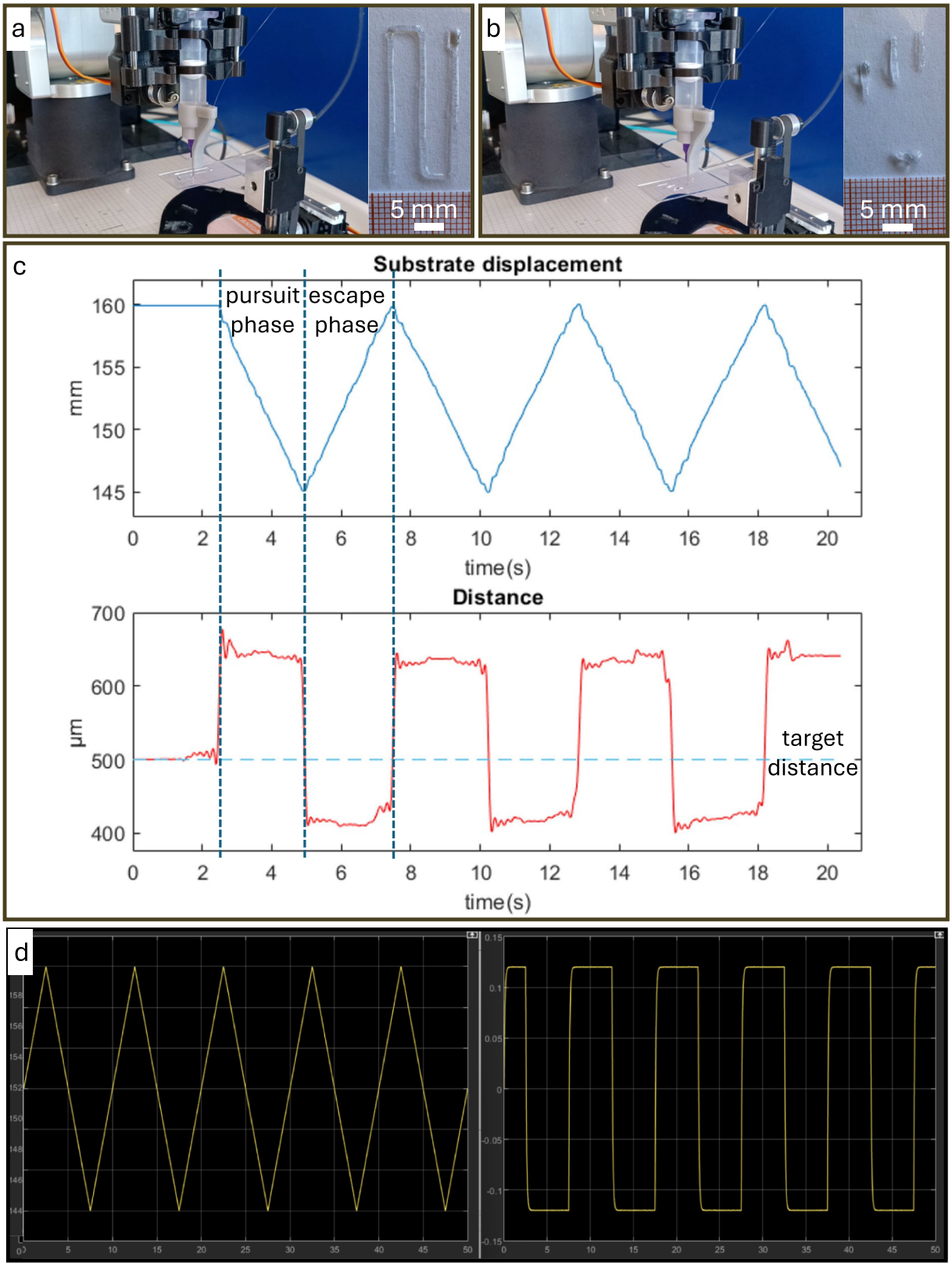

Fig. 3 a) Printing setup and results exploiting real-time robot compensation. - b) Printing setup and results with no compensation systems. - c) Position (z-coordinate) of the substrate as a function of time (top), measured distance between nozzle and substrate vs time (bottom) – d) results of the implemented Simulink® model

The choice of using a slide as the printing substrate also made it possible to verify the possibility of detecting distance variations from transparent substrates. This could have many advantages in the field of *in situ* or *in vitro* bioprinting since in both cases the most printed materials are hydrogels (GelMA, alginate or PEG-based hydrogels) characterised by high transparency. Having a distance detection system that does not detect transparent materials would make it impossible for the real-time distance correction system to work in the case of multilayer structures. In addition, *in vitro* bioprinting often uses transparent glass or plastic substrates (*e.g.,* Petri dishes, slides, multi-well) with non-perfectly planar geometries that require distance adaptation.

Tests onto static but *a priori* unknown surfaces resulted in regular prints with a line width standard deviation lower than 0.1 mm. As for the previous test onto a moving substrate, this is an acceptable result for bioprinting applications, where the desired resolution can range from 20 to 300 μm depending on the specific application [42], and this is immediately related to the accuracy of the deposited line width. Generally, we can consider acceptable a deviation of <20% from the needle diameter (target line width), considering both under and over-extrusion problems.

In the case of printing on the blue PLA surface (Fig. 4a), the distance value measured during the process was 508.7± 51.2 μm, demonstrating a remarkable ability to follow the profile throughout. In the case of printing on the black PLA surface (Fig. 4b), the distance value detected was 510.4±81.4 μm: although the result is satisfactory, both a greater variation from the desired distance and an increase in oscillations were observed throughout the printing phase. This could result from the lower reflective capacity of the surface, which could have caused a higher variability in the reading of the signal by the distance sensor. This issue might be minimised by including a localised lighting system close to the extrusion system (similar to [14]), which would ensure uniform brightness and better quality of the measured data even on darker substrates. Finally, the ability to print homogenous trajectories into a domed-bottomed petri dish (Fig. 4c) allowed us to verify the possibility of obtaining high-quality prints even in substrates that are inherently non-planar but commonly used in *in vitro* bioprinting applications. No statistically significant differences were found for the measured distance either (p-value > 0.05).

One of the main limitations of the proposed system concerns its current design, which involves a certain offset between the fiber-sensor and the extruder. This has led to the execution of non-planar trajectories with the end-effector kept vertical, in order to minimize possible collisions with the fiber in the event of rapid curvature changes during the execution of the trajectory. The current configuration, in which not all DOF of the robot are exploited, would allow for uniform printing on surfaces with a local curvature angle <45° (as proved in previous works [19, 26]), which would ensure good print quality (line width deviation <20% of the needle diameter). This could be resolved by changing the position of the fiber and placing it in direct contact with the needle, thereby minimizing the offset and thus the possible collision with the printing substrate, even in the case of high curvatures.

A key limitation at this stage is the method's clinical applicability. Our work establishes the technological foundation and shows a promising direction for future testing in real *in situ* bioprinting applications. However, to confirm its practical use, the OCT sensor's performance must also be evaluated in a physiological environment. For instance, an aqueous medium–with optical properties different from those of a glass slide–should be considered. This evaluation should account for potential variations in distance measurement accuracy, as well as the sensor's ability to maintain performance under more complex movement scenarios, such as irregular respiratory motion or sudden patient movements. It will also be essential to evaluate the system under a broader range of parameters (such as speed, pressure, and substrate distance) and with various materials (including GelMA, alginate, gelatin, and pectin). This will help demonstrate its suitability for effectively regenerating different types of biological tissues.

3.2 Experimental validation with the actuated end-effector

The use of the tool implemented to adapt the trajectories to the displacement of the substrate proved to be a functional method that enables printings that could not be performed without compensation systems (Fig. 5a-b). This approach resulted in less regularity in the printed lines, with a variability in line width of approximately 0.21 mm, thus 120 μm greater than the robot compensation system. Despite this, being able to use an actuated tool has considerable advantages since: (i) it requires the actuation of only one motor and not the correction of the entire robot kinematics; (ii) it can be connected as the end effector of any articulated robot, making the procedure more accessible even to systems that are not controllable in real-time. Comparing the time course of the substrate position with that of the nozzle-substrate distance detected during the compensated print (Fig. 5c), the same 'tracking' and 'fleeing' mechanism described in Section 3.2 can be observed: although the deviation from the desired distance is <100 μm in both phases, more variability is observed with respect to the robot compensation approach. These limitations, which result from the lower resolution of the developed belt-pulley mechanism (<50 μm) compared to that of the robot (1 μm), could be overcome by using servomotors with higher accuracy and a more rigid mechanical architecture.

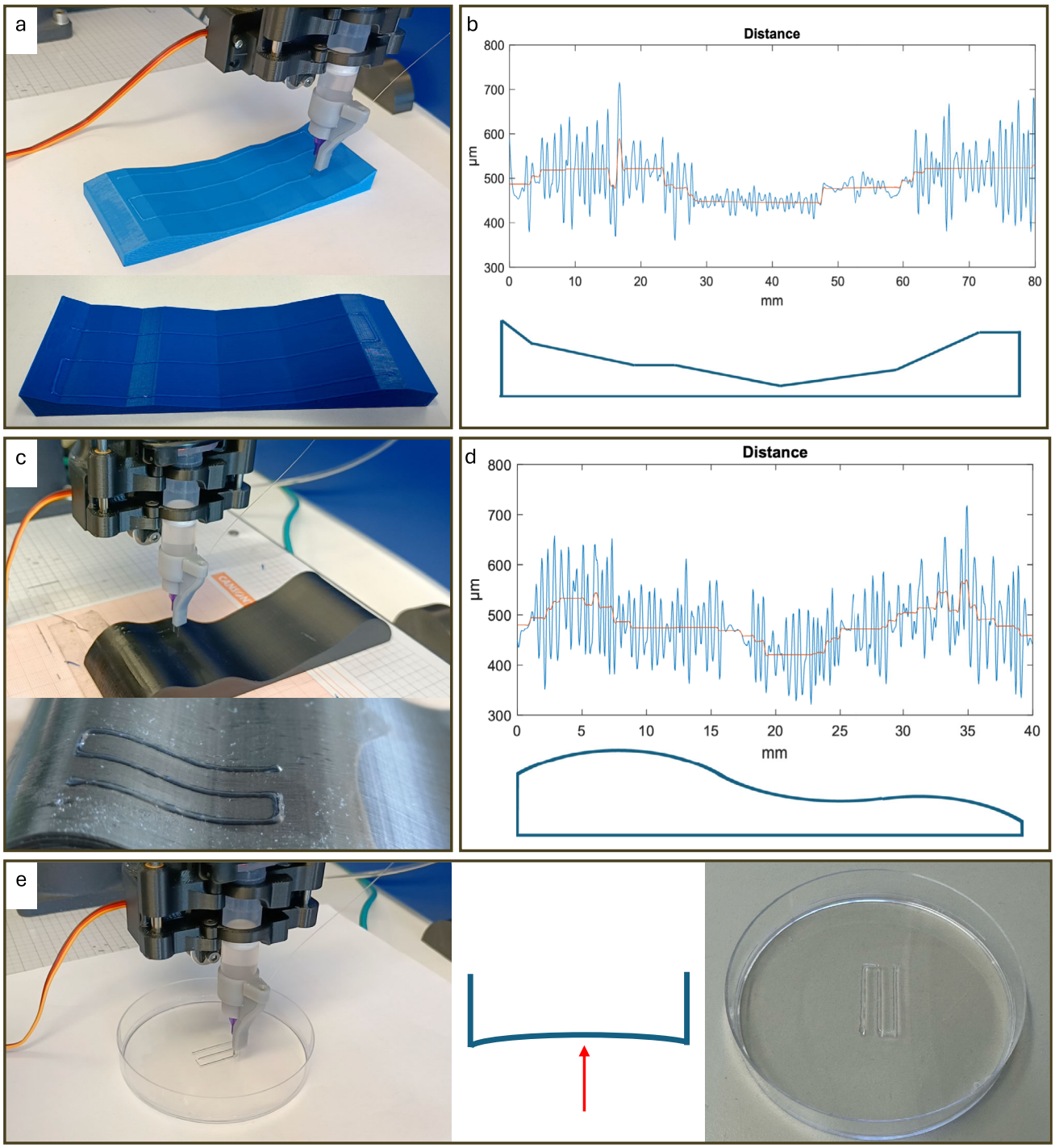

Fig. 4 a-b) Printing process and results on the blue PLA surface (left); distance value measured during printing (in blue the raw data, in red the data filtered by Total Variation Denoising (TVD) and the surface profile) (right). - c-d) Printing process and results on the black PLA surface; distance value measured during printing and the surface profile (right). A greater fluctuation of the distance value can be observed compared to a). - e) Printing process and results on a Petri dish with a convex bottom

Main experimental results, together with the environmental and printing parameters used for evaluating the sensing system performance and the obtained printing quality, are reported in Table 1 for both used approaches.

Considering the overall validation of the proposed system, this study serves as an initial step to demonstrate the feasibility of the proposed technology, providing a basis for future investigations under more physiologically relevant

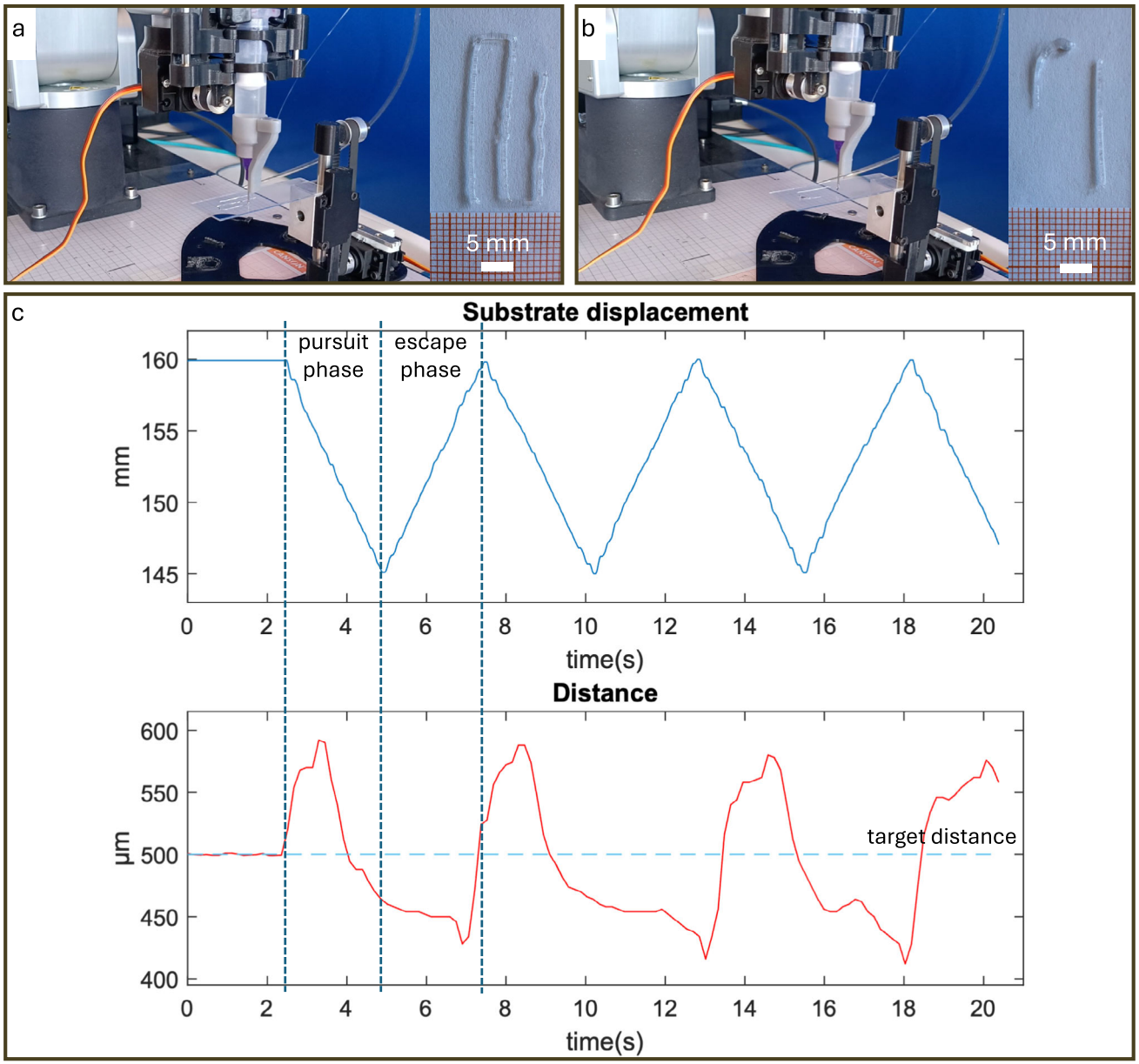

Fig. 5 a) Printing setup and serpentine trajectory realised by exploiting the implemented end-effector. - b) Printing setup and results obtained by not activating the compensation system. - c) Position (z-coordinate) of the substrate as a function of time (top), measured distance between nozzle and substrate (bottom)

Table 1 Environmental and printing parameters used for the experimental validation (values in mm; T=temperature, H=humidity, S=speed, P=pressure)

T=25°C - H=40% S=4mm/s - P=0.45 bar	Robot compensation		Actuated tool compensation	
	Line width	Distance	Line width	Distance
Moving glass slide	0.85 ± 0.09	Downward: 0.64 ± 0.01 Upward: 0.42 ± 0.02	0.85 ± 0.21	Downward: 0.65 ± 0.09 Upward: 0.47 ± 0.09
Unknown Blue PLA	0.84 ± 0.07	0.51 ± 0.05	//	//
Unknown Black PLA	0.85 ± 0.10	0.51 ± 0.08	//	//

conditions. While the current findings highlight its potential, further studies are required to evaluate performance under conditions that better mimic the complexity of *in vivo* environments. In addition, comprehensive biological validation will be essential to confirm the translational applicability of the approach and to ensure its robustness for potential clinical applications. This should be accompanied by an evaluation of the sterilisability of the entire printing system.

4 Conclusion

In this study, a robotic system for 3D printing capable of real-time compensating for unexpected movements or irregularities of the printing substrate was developed. Such a system could be promising, in the future, for efficient and safe *in situ* bioprinting procedures, where human tissues are inherently characterised by movements that can compromise both the quality and feasibility of the printing process. At the same time, the developed system makes it possible to improve print quality in all processes involving substrates with a non-perfectly planar shape, such as *in vitro* bioprinting, but can also be applied to any 3D printing process that takes place in environments characterised by strong vibrations, such as space stations or other moving vehicles. Two strategies for compensation were developed: one involving the adaptation of the robot's kinematics in order to adjust the position of the end-effector, and one involving the use of an actuated tool capable of moving and adapting to the position of the substrate. The results showed that the former allows better and more homogeneous prints to be obtained (deviation from the target line width < 100 μm, both onto moving and static *a priori* unknown substrates). Although it is necessary to improve the design of the actuated tool in order to obtain higher quality results (deviation from the target line width around 200 μm could not be acceptable depending on the application), this approach has the advantage of being computationally simple (it does not require recalculation of robot kinematics) and, above all, of being universally applicable to any printing platform. As discussed in the experimental section, a current limitation of the distance monitoring system is its positioning relative to the extruder. The current offset prevents its use on surfaces with high curvatures, as it could lead to a collision. A future upgrade will therefore be evaluated in which the fiber will be placed in direct contact with the needle to minimise the distance. Further studies will make it possible to optimize the control algorithm (e.g., to reduce the system latency during movements to and from the sensor) and the sensing system (e.g., local lighting system to improve sensor accuracy onto dark substrates, testing into a physiologically relevant environment) so as to be able to compensate for larger, irregular and faster movements, while also exploring printing with other materials and the realization of complex constructs. Ultimately, this work is intended as a preliminary study to demonstrate the effectiveness of the proposed technology, which may serve as a foundation for future investigations in more physiologically relevant scenarios, supported by rigorous biological validation.

Supplementary information

Supplementary videos are available to prove the ability of the real-time controlled robot, as well as the actuated tool, to print onto a moving transparent surface and onto *a priori* unknown substrates.

Supplementary Information The online version contains supplementary material available at https://doi.org/10.1007/s00170-025-16810-2.

Author Contributions All authors contributed to the study conception and design. Material preparation, data collection and analysis were performed by Andrea Guerra, Shakiba Davani, and Carlo Usai. Funding and resource acquisition were performed by Christos Boutopoulos, Tomasz Jüngst, and Gabriele Maria Fortunato. The first draft of the manuscript was written by Andrea Guerra and all authors commented on previous versions of the manuscript. All authors read and approved the final manuscript.

Funding This work found financial support from the Canadian Institutes of Health Research (#527176), the Fonds de la recherche en santé du Québec (FRQS) (#312263), and the Canada Foundation for Innovation (#43112), and was partially supported by the Italian Ministry of Education and Research (MUR) in the framework of the FoReLab and CrossLab projects (Departments of Excellence).

Declarations

Conflicts of Interest The authors have no relevant financial or non-financial interests to disclose.

References

1. Ahmadi M, Rahmatabadi D, Karimi A, Koohpayeh MHA, Hashemi R (2023) The role of additive manufacturing in the age of sustainable manufacturing 4.0. In: Sustainable manufacturing in industry 4.0: pathways and practices. Springer, Singapore, pp 57–78. https://doi.org/10.1007/978-981-19-7218-8_4
2. Zhu W, Ma X, Gou M, Mei D, Zhang K, Chen S (2016) 3d printing of functional biomaterials for tissue engineering. Curr Opin Biotechnol 40:103–112. https://doi.org/10.1016/j.copbio.2016.03.014
3. Langer R, Vacanti J (2015) Advances in tissue engineering. J Pediatr Surg 51(1):8–12. https://doi.org/10.1016/j.jpedsurg.2015.10.022
4. Mandrycky C, Wang Z, Kim K, Kim DH (2015) 3d bioprinting for engineering complex tissues. Biotechnol Adv 34(4):422–434. https://doi.org/10.1016/j.biotechadv.2015.12.011
5. De Maria C, Vozzi G, Moroni L (2017) Multimaterial, heterogeneous, and multicellular three-dimensional bioprinting. MRS Bull 42(8):578–584. https://doi.org/10.1557/mrs.2017.165

6. Dikyol C, Altunbek M, Bartolo P, Koc B (2021) Multimaterial bioprinting approaches and their implementations for vascular and vascularized tissues. Bioprinting 24:159. https://doi.org/10.1016/j.bprint.2021.e00159
7. Yan Y, Xiong Z, Hu Y, Wang S, Zhang R, Zhang C (2002) Layered manufacturing of tissue engineering scaffolds via multi-nozzle deposition. Mater Lett 57(18):2623–2628. https://doi.org/10.1016/s0167-577x(02)01339-3
8. Singh S, Choudhury D, Yu F, Mironov V, Naing MW (2019) In situ bioprinting-bioprinting from benchside to bedside? Acta Biomaterialia 101:14–25. https://doi.org/10.1016/j.actbio.2019.08.045
9. Nuutila K (2021) In vivo printing of growth factor-eluting adhesive scaffolds improves wound healing. Bioactive Mater 8:296–308. https://doi.org/10.1016/j.bioactmat.2021.06.030
10. Dong H (2023) Robotic-assisted automated in situ bioprinting. Int J Bioprint 9(1):629. https://doi.org/10.18063/ijb.v9i1.629
11. Samandari M, Mostafavi A, Quint J, Memić A, Tamayol A (2022) In situ bioprinting: intraoperative implementation of regenerative medicine. Trends Biotechnol 40(10):1229–1247. https://doi.org/10.1016/j.tibtech.2022.03.009
12. Li L, Shi J, Ma K, Jin J, Wang P, Liang H, Cao Y, Wang X, Jiang Q (2021) Robotic in situ 3d bio-printing technology for repairing large segmental bone defects. J Adv Res 30:75–84. https://doi.org/10.1016/j.jare.2020.11.011
13. Ozbolat IT, Chen H, Yu Y (2014) Development of 'multi-arm bioprinter'for hybrid biofabrication of tissue engineering constructs. Robot Comput-Integr Manuf. 30(3):295–304. https://doi.org/10.1016/j.rcim.2013.10.005
14. Fortunato GM, Batoni E, Pasqua I, Nicoletta M, Vozzi G, De Maria C (2023) Automatic photo-cross-linking system for robotic-based in situ bioprinting. ACS Biomater Sci Eng 9(12):6926–6934. https://doi.org/10.1021/acsbiomaterials.3c00898
15. Zennifer A, Manivannan S, Sethuraman S, Kumbar SG, Sundaramurthi D (2022) 3d bioprinting and photocrosslinking: emerging strategies & future perspectives. Biomater Adv 134:112576. https://doi.org/10.1016/j.msec.2021.112576
16. Ma K, Zhao T, Yang L, Wang P, Jin J, Teng H, Xia D, Zhu L, Li L, Jiang Q et al (2020) Application of robotic-assisted in situ 3d printing in cartilage regeneration with Hama hydrogel: an in vivo study. J Adv Res 23:123–132. https://doi.org/10.1016/j.jare.2020.01.010
17. Fortunato GM, Rossi G, Bonatti AF, De Acutis A, Mendoza-Buenrostro C, Vozzi G, De Maria C (2021) Robotic platform and path planning algorithm for in situ bioprinting. Bioprinting 22:00139. https://doi.org/10.1016/j.bprint.2021.e00139
18. Urhal P, Weightman A, Diver C, Bartolo P (2019) Robot assisted additive manufacturing: a review. Robot Comput-Integr Manuf 59:335–345. https://doi.org/10.1016/j.rcim.2019.05.005
19. Fortunato GM, Sigismondi S, Nicoletta M, Condino S, Montemurro N, Vozzi G, Ferrari V, De Maria C (2023) Analysis of the robotic-based in situ bioprinting workflow for the regeneration of damaged tissues through a case study. Bioengineering 10(5):560. https://doi.org/10.3390/bioengineering10050560
20. Fortunato G.M, Molisani M, Vozzi G, De Maria C (2023) Extrusion control strategy for robotic-based in situ bioprinting. In: Convegno Nazionale di Bioingegneria. Patron Editore Srl, Italy
21. Kalan S, Chauhan S, Coelho RF, Orvieto MA, Camacho IR, Palmer KJ, Patel VR (2010) History of robotic surgery. J Robot Surg 4:141–147. https://doi.org/10.1007/s11701-010-0202-2
22. Shim J-H, Lee J-S, Kim JY, Cho D-W (2012) Bioprinting of a mechanically enhanced three-dimensional dual cell-laden construct for osteochondral tissue engineering using a multi-head tissue/organ building system. J Micromech Microeng 22(8):085014. https://doi.org/10.1088/0960-1317/22/8/085014
23. Friedman D.C, Dosher J, Kowalewski T, Rosen J, Hannaford B (2007) Automated tool handling for the trauma pod surgical robot. In: Proceedings 2007 IEEE International Conference on Robotics and Automation. pp 1936–1941. https://doi.org/10.1109/ROBOT.2007.363605
24. Guerra A, Fortunato GM, Batoni E, Vozzi G, De Maria C (2025) Multi-material and multi-scale platform for robotic based in situ bioprinting. Res Eng 104219. https://doi.org/10.1016/j.rineng.2025.104219
25. Zhao W, Chen H, Zhang Y, Zhou D, Liang L, Liu B, Xu T (2022) Adaptive multi-degree-of-freedom in situ bioprinting robot for hair-follicle-inclusive skin repair: a preliminary study conducted in mice. Bioeng Translat Med 7(3):10303. https://doi.org/10.1002/btm2.10303
26. Fortunato GM, Batoni E, Bonatti AF, Vozzi G, De Maria C (2022) Surface reconstruction and tissue recognition for robotic-based in situ bioprinting. Bioprinting 26:00195. https://doi.org/10.1016/j.bprint.2022.e00195
27. Dockter R, Sweet R, Kowalewski T (2014) A fast, low-cost, computer vision approach for tracking surgical tools. In: 2014 IEEE/RSJ International Conference on Intelligent Robots and Systems. pp 1984–1989. https://doi.org/10.1109/IROS.2014.6942826
28. Ozbolat IT, Yu Y (2013) Bioprinting toward organ fabrication: challenges and future trends. IEEE Trans Biomed Eng 60(3):691–699. https://doi.org/10.1109/TBME.2013.2243912
29. O'Neill JJ, Johnson RA, Dockter RL, Kowalewski TM (2017) 3d bioprinting directly onto moving human anatomy. In: 2017 IEEE/RSJ International Conference on Intelligent Robots and Systems (IROS). pp 934–940. https://doi.org/10.1109/IROS.2017.8202257
30. Fortunato GM, Bonatti AF, Batoni E, Macaluso R, Vozzi G, De Maria C (2022) Motion compensation system for robotic based in situ bioprinting to balance patient physiological movements. Bioprinting 28:00248. https://doi.org/10.1016/j.bprint.2022.e00248
31. Haase S, Forman C, Kilgus T, Bammer R, Maier-Hein L, Hornegger J (2013) Tof/rgb sensor fusion for 3-d endoscopy. Curr Med Imaging Rev 9(2):113–119. https://doi.org/10.2174/1573405611309020006
32. Maier-Hein L, Mountney P, Bartoli A, Elhawary H, Elson D, Groch A, Kolb A, Rodrigues M, Sorger J, Speidel S et al (2013) Optical techniques for 3d surface reconstruction in computer-assisted laparoscopic surgery. Med Image Anal 17(8):974–996. https://doi.org/10.1016/j.media.2013.04.003
33. Phillips BT, Allder J, Bolan G, Nagle RS, Redington A, Hellebrekers T, Borden J, Pawlenko N, Licht S (2020) Additive manufacturing aboard a moving vessel at sea using passively stabilized stereolithography (sla) 3d printing. Addit Manuf 31:100969. https://doi.org/10.1016/j.addma.2019.100969
34. Chan K, Arumugam A, Markham C, Jenson R, Wu H-W, Wong S (2023) The development of a 3d printer-inspired, microgravity-compatible sample preparation device for future use inside the international space station. Micromachines 14(5):937. https://doi.org/10.3390/mi14050937
35. Truby RL, Lewis JA (2016) Printing soft matter in three dimensions. Nature 540(7633):371–378. https://doi.org/10.1038/nature21003
36. Zhu Z, Guo S-Z, Hirdler T, Eide C, Fan X, Tolar J, McAlpine MC (2018) 3d printed functional and biological materials on moving freeform surfaces. Adv Mater 30(23):1707495. https://doi.org/10.1002/adma.201707495
37. Armstrong AA, Alleyne AG, Johnson AJW (2020) 1d and 2d error assessment and correction for extrusion-based bioprinting using process sensing and control strategies. Biofabrication 12(4):045023. https://doi.org/10.1088/1758-5090/aba8ee

38. Kucukdeger E, Johnson BN (2023) Closed-loop controlled conformal 3d printing on moving objects via tool-localized object position sensing. J Manuf Process 89:39–49. https://doi.org/10.1016/j.jmapro.2023.01.020
39. Levin AA, Karalkin PA, Koudan EV, Senatov FS, Parfenov VA, Lvov VA, Petrov SV, Pereira FD, Kovalev AV, Osidak EO et al (2023) Commercial articulated collaborative in situ 3d bioprinter for skin wound healing. Int J Bioprint 9(2):675. https://doi.org/10.18063/ijb.v9i2.675
40. Abid A, Mittal S, Boutopoulos C (2020) Etching-enabled extreme miniaturization of graded-index fiber-based optical coherence tomography probes. J Biomed Opt 25(3):032006–032006. https://doi.org/10.1117/1.jbo.25.3.032006
41. Boer JF (2015) Spectral/fourier domain optical coherence tomography. In: Optical Coherence Tomography. Springer, Cham, pp 165–193. https://doi.org/10.1007/978-3-319-06419-2_6
42. Miri AK, Mirzaee I, Hassan S, Oskui SM, Nieto D, Khademhosseini A, Zhang YS (2019) Effective bioprinting resolution in tissue model fabrication. Lab Chip 19(11). https://doi.org/10.1039/c8lc01037d

Authors and Affiliations

Andrea Guerra[1,2] · Shakiba Davani[3] · Carlo Usai[1,2] · Tomasz Jüngst[4] · Christos Boutopoulos[3] · Gabriele Maria Fortunato[1,2]

✉ Gabriele Maria Fortunato
gabriele.fortunato@unipi.it

Andrea Guerra
andrea.guerra1@phd.unipi.it

Shakiba Davani
shakiba.davani@umontreal.ca

Carlo Usai
c.usai1@studenti.unipi.it

Tomasz Jüngst
tomasz.juengst@uni-wuerzburg.de

Christos Boutopoulos
christos.boutopoulos@umontreal.ca

1 Department of Information Engineering, University of Pisa, Largo Lucio Lazzarino 1, Pisa 56122, Italy

2 Research Centre "E. Piaggio", University of Pisa, Largo Lucio Lazzarino 1, Pisa 56122, Italy

3 Department of Ophthalmology and Institute of Biomedical Engineering, University of Montréal, Pavillon Roger-Gaudry, Edouard Montpetit Blvd, Montreal 2900, Quebec H3T 1J4, Canada

4 Department of Functional Materials in Medicine and Dentistry, University of Würzburg, Pleicherwall 2, Würzburg 97070, Germany